NOISE-ROBUST SPATIAL PREPROCESSING PRIOR TO ENDMEMBER EXTRACTION FROM HYPERSPECTRAL DATA

Gabriel Martín, Antonio Plaza

Hyperspectral Computing Laboratory
University of Extremadura
E-10071 Cáceres, Spain
E-mail: {gamahefpi, aplaza}@unex.es

Maciel Zortea

Department of Mathematics and Statistics
University of Tromsø
N-9037 Tromsø, Norway
E-mail: maciel.zortea@hyperinet.eu

ABSTRACT

This paper develops a noise-robust spatial preprocessing module which can be used prior to spectral unmixing of remotely sensed hyperspectral images. The method first derives a spatial homogeneity index which is relatively insensitive to the noise present in the original hyperspectral data. Then, it fuses this index with a spectral-based classification, obtaining a set of pure regions which are used to guide the unmixing process. An experimental comparison of the proposed method with other spatial-spectral unmixing approaches is conducted using both synthetic and real hyperspectral data collected by the Airborne Visible Infra-Red Imaging Spectrometer (AVIRIS). Our experiments indicate that spectral unmixing can benefit from the proposed pre-processing approach, in particular, when the noise level present in the original hypespectral scene is relatively high.

1. INTRODUCTION

Spectral unmixing is an important task in remotely sensed hyperspectral data exploitation [1]. Let us assume that a remotely sensed hyperspectral scene with n bands is denoted by $\mathbf{X}$, in which the pixel at the discrete, spatial coordinates (i, j) of the scene is represented by a feature vector given by $\mathbf{X}(i,j) = [x_1(i,j), x_2(i,j), \cdots, x_n(i,j)] \in \Re^n$, and $\Re$ denotes the set of real numbers corresponding to the pixel's spectral response $x_k(i,j)$ at sensor channels $k = 1, \ldots, n$. Under the linear mixture model assumption, each (possibly mixed) pixel vector in the original scene can be modeled using the following expression:

$$\mathbf{X}(i,j) = \sum_{z=1}^{p} \Phi_z(i,j) \cdot \mathbf{E}_z + \mathbf{n}(i,j), \qquad (1)$$

where $\mathbf{E}_z$ denotes the spectral response of the z-th pure spectral signature (*endmember*) participating in the mixture, $\Phi_z(i,j)$ is a scalar value designating the fractional abundance of the z-th endmember at pixel $\mathbf{X}(i,j)$, p is the total number of endmembers, and $\mathbf{n}(i,j)$ is a noise vector. Two physical constrains are generally imposed into the model described in (1), these are the abundance non-negativity constraint (ANC), i.e., $\Phi_z(i,j) \geq 0$, and the abundance sum-to-one constraint (ASC), i.e., $\sum_{z=1}^{p} \Phi_z(i,j) = 1$ [2].

Over the few years, many techniques have been developed for spectral-based endmember extraction [3] but only a few methods have been designed under the assumption that spatial information can help in the process of extracting spectral endmembers. Techniques include automatic morphological endmember extraction (AMEE) [4], spatial-spectral endmember extraction (SSEE) [5], spatial preprocessing (SPP) using a sliding-window approach [6], and a region-based spatial preprocessing (RBSPP) approach [7]. The first two approaches are endmember extraction algorithms themselves, while the latter two approaches are preprocessing modules that can be combined with any other spectral-based endmember extraction algorithm. Although these approaches have been shown in previous work to be effective in spatial-spectral characterization prior to spectral unmixing, their performance is generally sensitive to noise.

In this work, we propose a noise-robust spatial preprocessing (NRSPP) module which can be used in combination with available endmember extraction algorithms. The method first derives a spatial homogeneity index which is relatively insensitive to the noise present in the original hyperspectral data. Then, it fuses this index with a spectral-based classification, obtaining a set of pure regions which are used to guide the endmember searching process. The remainder of the abstract is organized as follows. In section 2, we describe the proposed method in step-by-step fashion using a synthetic hyperspectral image to illustrate the outcome of each step. In section 3, we provide an experimental comparison of the proposed method with other spatial-spectral approaches such as AMEE, SSEE, SPP and RBSPP using both synthetic and real hyperspectral data collected by the Airborne Visible Infra-Red Imaging Spectrometer (AVIRIS) [8]. This section also includes future research lines.

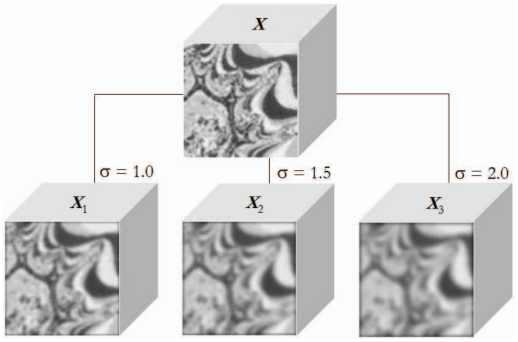

Fig. 2. Gaussian filtering of the synthetic hyperspectral image in Fig. 1

2. NOISE-ROBUST SPATIAL PREPROCESSING (NRSPP)

In order to describe the proposed approach in step-by-step fashion, we use a 100×100-pixel synthetic hyperspectral scene. Fig. 1 shows the spectra of the U.S. Geological Survey (USGS)[1] signatures used in the simulation of the synthetic scene. The abundance maps associated to each reference USGS signature are also displayed in Fig. 1, where black color indicates 0% abundance of the corresponding mineral, white color indicates 100% abundance of the mineral. The fractional abundances in each pixel of the scene sum to unity. Zero-mean Gaussian noise was added in different signal to noise ratios (SNRs) –from 30:1 to 110:1– to simulate contributions from ambient and instrumental sources, following the procedure described in [9]. The proposed NRSPP method can be described in step-by-step fashion as follows:

1. *Multi-scale Gaussian filtering*. First, we apply multidimensional Gaussian filtering using different values of parameter σ, which results in different filtered versions $\mathbf{X}_1, \mathbf{X}_2, \cdots, \mathbf{X}_l$ of the original hyperspectral image $\mathbf{X}$. Here, parameter l determines the number of levels, and higher σ values lead to more spatial smoothing. Fig. 2 shows the outcome of applying Gaussian filtering (with $l = 3$) using different values of σ for the synthetic image simulated with SNR=70:1.

2. *Spatial homogeneity calculation*. Next, we calculate the root mean square error (RMSE) between the original image $\mathbf{X}$ and each of the filtered images in the set $\{\mathbf{X}_i\}_{i=1}^{l}$. Figs. 3(a-c) respectively show the outcome of calculating $\Delta_1 = \text{RMSE}(\mathbf{X}, \mathbf{X}_1)$, $\Delta_2 = \text{RMSE}(\mathbf{X}, \mathbf{X}_2)$ and $\Delta_3 = \text{RMSE}(\mathbf{X}, \mathbf{X}_3)$ for the synthetic image with SNR=70:1. Then, for each pixel at spatial coordinates (i, j) in the hyperspectral image $\mathbf{X}$, we calculate a spatial homogeneity index as the average value of the corresponding values in $\{\Delta_i\}_{i=1}^{l}$, *i.e.*, $S(i,j) = \frac{1}{l}\sum_{i=1}^{l} \Delta_i(i,j)$. Figs. 3(d-h) respectively show the spatial homogeneity images obtained for the synthetic image with SNR values ranging between 30:1 and 110:1. As shown by Figs. 3(d-h), the spatial homogeneity calculation is robust in the presence of noise.

3. *Spectral classification*. In parallel to the first two steps, we perform a spectral-based unsupervised classification of $\mathbf{X}$. Here, we simply used the ISODATA algorithm applied to a transformed version of the original image obtained using the minimum noise fraction (MNF) transform [10], where the number of components retained was set to p, the number of endmembers in the input data, estimated using the virtual dimensionality (VD) concept [11]. For the ISODATA algorithm, the minimum number of classes was set to p and the maximum number of classes was set to $2p$, which empirically resulted in good results. Fig. 3(i) shows the spectral classification result for the synthetic image with SNR=70:1.

4. *Fusion*. For each cluster in the spectral classification map, a subset of spatially homogeneous pixels are selected. Parameter $\alpha \in [0, 100]$ defines the percentage of pixels that will be selected per cluster. For selection, pixels are ranked according to increasing values of $S(i,j)$. The selected pixels for each cluster are now averaged, then we apply the orthogonal subspace projection (OSP) algorithm [9] over the averaged signatures in order to select the most extreme clusters and remove the clusters with mixed pixels. Fig. 3(j-n) shows the clusters obtained from the image with SNR=70:1 after considering values of α from 50 to 90.

Finally, endmember extraction is applied to the retained pixels after the NRSPP procedure above by assuming that, every time an endmember pixel is selected from a certain cluster, all remaining pixels in the same cluster are excluded from the endmember searching process. The outcome is a set of p endmembers (extracted in this work using the OSP algorithm).

Table 1. SA scores measured after applying several endmember extraction algorithms to the synthetic scene in Fig. 1.

Algorithm	SNR=30:1	SNR=50:1	SNR=70:1	SNR=90:1	SNR=110:1
OSP	2.001	**0.275**	**0.170**	**0.166**	**0.177**
SPP+OSP	**1.977**	0.368	0.237	0.232	0.232
RBSPP+OSP	2.023	0.392	0.378	0.308	0.388
NRSPP+OSP	1.996	0.291	0.181	0.179	0.190
AMEE	6.170	5.133	4.362	4.361	4.361
SSEE	2.002	0.554	0.235	0.850	0.242

3. EXPERIMENTAL RESULTS

Two different metrics have been used as performance indicators. The first one is the spectral angle (SA) [1] between each

[1] http://speclab.cr.usgs.gov/spectral-lib.html

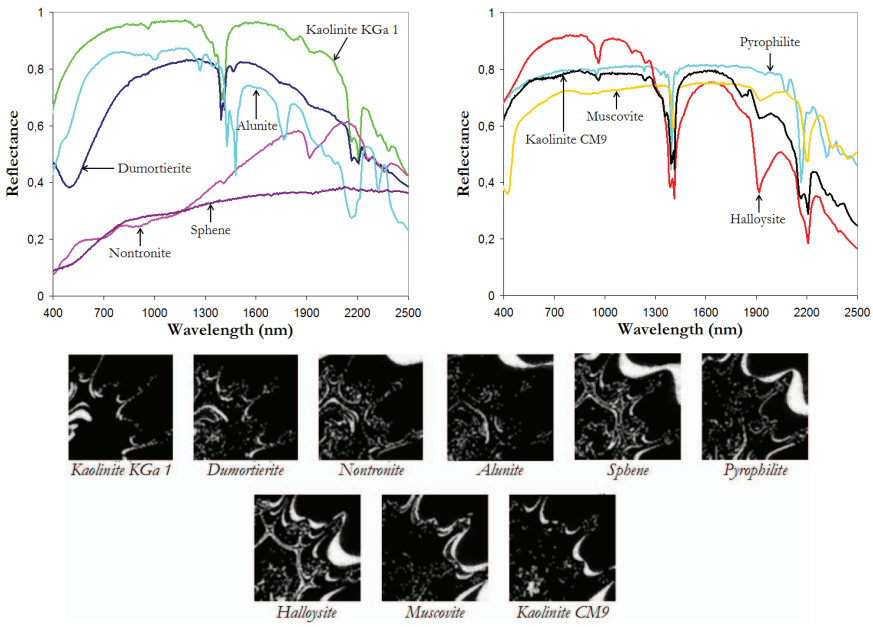

Fig. 1. USGS signatures (top) and fractional abundances (bottom) considered for generating a synthetic hyperspectral scene.

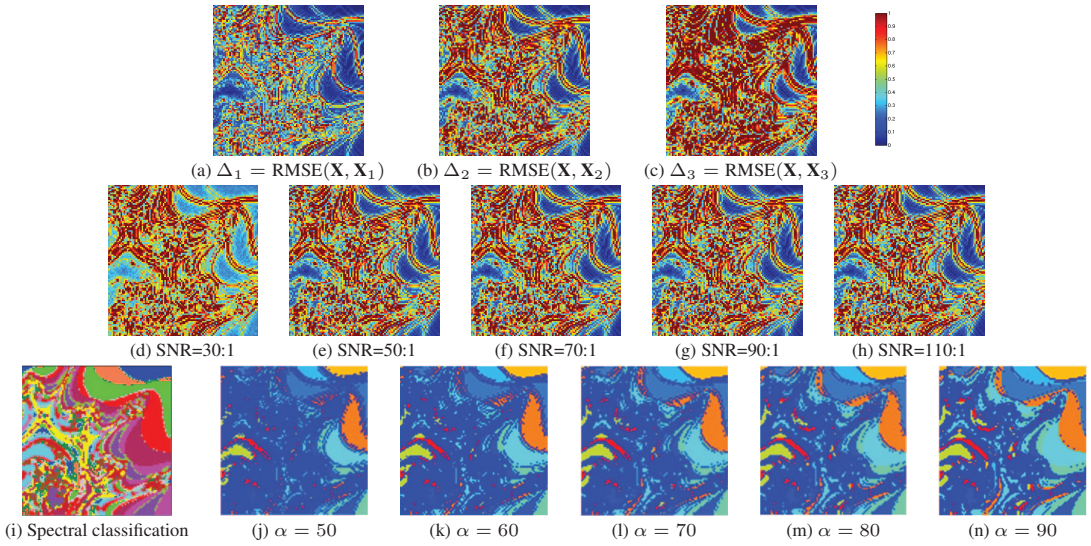

Fig. 3. (a) RMSE($\mathbf{X}$,$\mathbf{X}_1$) for the image with SNR=70:1. (b) RMSE($\mathbf{X}$,$\mathbf{X}_2$) for the image with SNR=70:1. (c) RMSE($\mathbf{X}$,$\mathbf{X}_3$) for the image with SNR=70:1. (d-h) Spatial homogeneity scores for different SNR values. (i) Spectral classification of the image with SNR=70:1. (j-n) Regions obtained after fusing (f) and (i) considering different values of α.

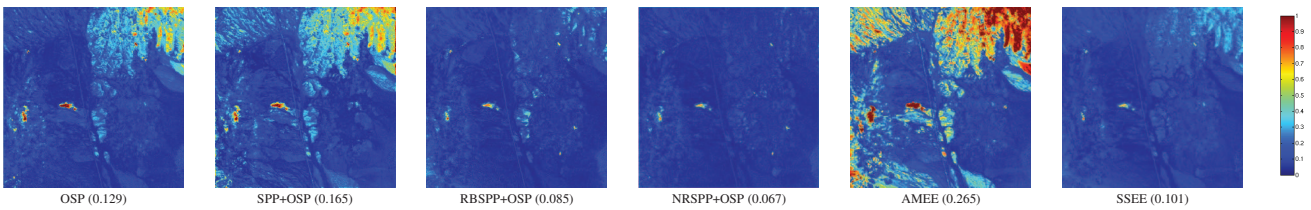

Fig. 4. Errors measured for various endmember extraction algorithms after reconstructing the AVIRIS Cuprite scene.

Table 2. RMSE scores measured after applying several endmember extraction algorithms to the synthetic scene in Fig. 1.

Algorithm	SNR=30:1	SNR=50:1	SNR=70:1	SNR=90:1	SNR=110:1
OSP	0.3469	0.0372	0.0084	0.0066	0.0063
SPP+OSP	0.3498	0.0423	0.0149	0.0132	0.0132
RBSPP+OSP	0.3469	0.0372	0.0087	0.0070	0.0059
NRSPP+OSP	**0.3464**	**0.0363**	**0.0068**	**0.0050**	**0.0047**
AMEE	0.4767	0.3294	0.3190	0.3187	0.3187
SSEE	0.3472	0.0439	0.0075	0.0282	0.0090

extracted endmember and the set of available USGS ground-truth spectral signatures. The lower the SA, the better the result. The second one is the RMSE between the original and a reconstructed version of the hyperspectral scene [6], obtained using the ASC and ANC-constrained linear mixture model in (1). Table 1 shows the SA scores (in degrees) between the reference USGS mineral spectra and their corresponding endmember pixels extracted by several endmember extraction algorithms from the synthetic scene in Fig. 1 simulated with different SNR values. Parameter values have been carefully optimized for all considered methods. As shown by Table 1, the NRSPP does not provide the best SA scores but always provides very competitive results for all considered SNR values. On the other hand, Table 2 shows the RMSE scores after reconstructing the synthetic scene (simulated with different SNR values) using the endmembers extracted by several methods. Table 2 indicates that the NRSPP provides the best overall results (lower RMSE values) regardless of the considered SNR. Finally, Fig. 4 shows the error maps obtained after reconstructing the well-known AVIRIS Cuprite scene[2] using $p = 19$ endmembers extracted by different methods (this value of p was estimated with the VD concept). Fig. 4 reveals that the application of NRSPP as preprocessing results in more robust reconstruction results than those found by using other methods.

4. CONCLUSIONS AND FUTURE RESEARCH

We have developed a new spatial-spectral pre-processing method which can be used prior to endmember extraction and spectral unmixing of remotely sensed hyperspectral images. The proposed method shows some advantages over other existing approaches, in particular, when the noise level in the hyperspectral data is relatively high. Additional experiments exploring the combined use of pre-screening methods to filter out mixed pixels with the proposed method will be conducted in future research.

5. REFERENCES

[1] N. Keshava and J. F. Mustard, "Spectral unmixing," *IEEE Signal Processing Magazine*, vol. 19, no. 1, pp. 44–57, 2002.

[2] D. Heinz and C.-I Chang, "Fully constrained least squares linear mixture analysis for material quantification in hyperspectral imagery," *IEEE Transactions on Geoscience and Remote Sensing*, vol. 39, pp. 529–545, 2000.

[3] A. Plaza, P. Martinez, R. Perez, and J. Plaza, "A quantitative and comparative analysis of endmember extraction algorithms from hyperspectral data," *IEEE Transactions on Geoscience and Remote Sensing*, vol. 42, no. 3, pp. 650–663, 2004.

[4] A. Plaza, P. Martinez, R. Perez, and J. Plaza, "Spatial/spectral endmember extraction by multidimensional morphological operations," *IEEE Transactions on Geoscience and Remote Sensing*, vol. 40, no. 9, pp. 2025–2041, 2002.

[5] D. M. Rogge, B. Rivard, J. Zhang, A. Sanchez, J. Harris, and J. Feng, "Integration of spatial–spectral information for the improved extraction of endmembers," *Remote Sensing of Environment*, vol. 110, no. 3, pp. 287–303, 2007.

[6] M. Zortea and A. Plaza, "Spatial preprocessing for endmember extraction," *IEEE Transactions on Geoscience and Remote Sensing*, vol. 47, pp. 2679–2693, 2009.

[7] G. Martin and A. Plaza, "Region-based spatial preprocessing for endmember extraction and spectral unmixing," *Submitted to IEEE Geoscience and Remote Sensing Letters*, 2010.

[8] R. O. Green, M. L. Eastwood, C. M. Sarture, T. G. Chrien, M. Aronsson, B. J. Chippendale, J. A. Faust, B. E. Pavri, C. J. Chovit, M. Solis, et al., "Imaging spectroscopy and the airborne visible/infrared imaging spectrometer (AVIRIS)," *Remote Sensing of Environment*, vol. 65, no. 3, pp. 227–248, 1998.

[9] J. C. Harsanyi and C.-I Chang, "Hyperspectral image classification and dimensionality reduction: An orthogonal subspace projection," *IEEE Transactions on Geoscience and Remote Sensing*, vol. 32, no. 4, pp. 779–785.

[10] A. A. Green, M. Berman, P. Switzer, and M. D. Craig, "A transformation for ordering multispectral data in terms of image quality with implications for noise removal," *IEEE Transactions on Geoscience and Remote Sensing*, vol. 26, pp. 65–74, 1988.

[11] C.-I Chang and Q. Du, "Estimation of number of spectrally distinct signal sources in hyperspectral imagery," *IEEE Transactions on Geoscience and Remote Sensing*, vol. 42, no. 3, pp. 608–619, 2004.

[2] http://aviris.jpl.nasa.gov/html/aviris.freedata.html